JOURNAL OF SCIENCE TECHNOLOGY AND EDUCATION 12(4), DECEMBER, 2024
ISSN: 2277-0011; Journal homepage: www.atbuftejoste.com.ng

Investigation of ZnS Nanoparticles as a Cadmium-Free Buffer Layer for CZTSe Solar Cells

[1]Hassan Mustapha Junaidu, [1]Musa Bello, [2]Muhammad Yusuf Onimisi, [2]Bala Dennis, [2]Haruna Ali, [2]Rabiu Abubakar Tafida
[1]*Department of Science Education,*
Faculty of Technology Education Abubakar Tafawa Balewa University Bauchi, Nigeria
[2]*Department of Physics, Faculty of Science, Nigeria Defense Academy, Kaduna Nigeria*

ABSTRACT
This research investigates the implementation of Zinc Sulfide (ZnS) buffer layers in Copper Zinc Tin Selenide (CZTSe) thin-film solar cells as an eco-friendly alternative to conventional Cadmium Sulfide (CdS) buffer layers. CZTSe, a promising material for thin-film photovoltaic applications, possesses favorable optoelectronic properties, while CdS presents environmental concerns due to its toxicity. This study explores the feasibility of ZnS as a non-toxic and potentially superior substitute, leveraging its compatibility with CZTSe and advantageous band alignment. The investigation involves systematic variation of ZnS thin film thicknesses and structural characteristics to optimize its properties. Structural, morphological, and optical analyses using techniques such as X-ray diffraction (XRD), scanning electron microscopy (SEM), and UV-Vis spectroscopy reveal promising results. XRD analysis confirms the formation of ZnS thin films with wurtzite crystal structure, while SEM imaging depicts well-defined nanostructures. UV-Vis spectroscopy demonstrates tunable optical bandgaps with varying ZnS film thicknesses. Additionally, electrical characterization through current-voltage (IV) measurements reveals promising conductivity properties of ZnS films. The integration of ZnS buffer layers into CZTSe solar cell devices exhibits encouraging performance, albeit with lower efficiency compared to CdS-based counterparts. Despite challenges such as reduced short-circuit current, the results indicate the potential of ZnS as a buffer layer material, warranting further optimization and exploration. Overall, this study contributes to advancing the understanding of ZnS/CZTSe interfaces and their implications for thin-film photovoltaic device performance, paving the way for the development of more efficient and environmentally sustainable solar energy technologies.

ARTICLE INFO
Article History
Received: September, 2024
Received in revised form: November, 2024
Accepted: November, 2024
Published online: December, 2024

KEYWORDS
CZTSe, ZnS nanoparticles, Buffer Layer, Thin-Film Solar Cells, Cadmium-Free, Photovoltaics.

INTRODUCTION

Copper Zinc Tin Sulfide (CZTS) emerged as a promising photovoltaic material in 1988 at Shishu University, Japan. Ito and Nakazawa (1988) fabricated a p-type CZTS polycrystalline film on glass using sputtering, achieving an absorption coefficient exceeding 10^4 cm^{-1} and and a direct bandgap of 1.45 eV (Ito & Nakazawa, 1988). This discovery paved the way for research into quaternary CZTS-related semiconductors, including CZTSe (Friedlmeier et al., 1997) and CZTSSe have been synthesized for semiconductor applications. The exploration of CZTSe (Copper-Zinc-Tin-Selenide) for photovoltaic applications began in the early 2000s, with a focus on nanoparticle synthesis and characterization (Shi et al., 2011).

Corresponding author: Hassan Mustapha Junaidu
✉ hassanmustapha0@gmail.com
Department of Science Education, Faculty of Technology Education Abubakar Tafawa Balewa University Bauchi, Nigeria.
© 2024. Faculty of Technology Education. ATBU Bauchi. All rights reserved

JOURNAL OF SCIENCE TECHNOLOGY AND EDUCATION 12(4), DECEMBER, 2024
ISSN: 2277-0011; Journal homepage: www.atbuftejoste.com.ng

CZTSe forms through the incorporation of zinc into the lattice of copper-tin-selenium ternary compounds, resulting in quaternary structures like $Cu_2ZnSnSe_4$ (Lai et al., 2022). Li et al., (2015) described the formation mechanism, involving a progressive consumption of the alloy layer with a copper-tin top and zinc bottom, transforming into CZTSe from the surface downwards. CZTSe has gained significant attention as a thin-film solar cell absorber material due to its non-toxic constituents, abundant elements, and high production capacity (Huang et al., 2014). This material boasts a direct bandgap of 1.0 eV, a high optical absorption coefficient, and low cost, making it a strong candidate for high-efficiency solar cells (Lai et al., 2020).

The toxicity of cadmium in CdS buffer layers presents a significant environmental concern (Wang et al., 2021). ZnS has emerged as a non-toxic alternative for CdS in solar cell buffer layers. Studies have demonstrated successful replacement of CdS with ZnS in various solar cell types, including $Cu(In,Ga)(S,Se)_2$ (CIGS) and Cu_2ZnSnS_4 (CZTS), while maintaining or even improving performance (Barman & Kalita, 2020; Chantana et al., 2018; Rodríguez et al., 2016; Sara et al., 2018; Zhang et al., 2016). ZnS is a favorable candidate due to its wide bandgap, aligning well with its desired electronic and optical properties for buffer layer applications (Chantana et al., 2017, 2018). The wide bandgap energy and non-toxic nature of ZnS make it a promising alternative for buffer layers in CZTS-based solar cells (Yassine et al., 2022).

Sputtered ZnS thin films have been reported to possess a bandgap ranging from 3.3 to 3.4 eV (Bashar et al., 2020). Similarly, Kumar & Arora (2021) proposed ZnS as a potential buffer layer substitute for CdS in $Cu(In,Ga)Se_2$ solar cells, aiming for Cd-free devices. Wang et al. (2021) emphasized the widespread use of Zn(O,S) films as Cd-free buffer layers for kesterite solar cells due to their cost-effectiveness and environmental benefits. Additionally, Delgado-Sanchez & Lillo-Bravo (2022) highlighted ZnS as the most promising alternative to CdS, possessing similar electronic and optical properties, further solidifying its potential as a replacement.

Researchers have explored various techniques for ZnS nanoparticle synthesis. These include plasma-assisted synthesis with precursor exposure to oxygen plasma (Primc et al., 2021), hydrothermal processes involving X-ray diffraction and spectroscopy techniques (Wirunchit & Koetniyom, 2023), hydrometallurgical methods using acetic acid as a leaching agent (Diguna et al., 2021), and flame-assisted spray pyrolysis methods (Nemade & Waghuley, 2016). ZnS has been deposited as thin film by various methods such as chemical bath deposition (CBD), sol-gel technique, and pulsed-laser deposition (PLD) (Eisa & Ahmed, 2021; Goktas et al., 2012; Hsieh et al., 2011; Mohammed, 2021; Opasanont et al., 2015). These methods have been extensively used to investigate the structural, optical, and electrical properties of ZnS thin films. Motivated by the aforementioned advantages and research gaps, this study aims to investigate the potential of ZnS nanoparticles.

EXPERIMENTAL DETAILS

Reagents used for the Synthesis of ZnS

Hydrothermal method as reported by Zhao & Zhang (2012), was used for the purpose of synthesizing the ZnS nanostructures. The precursors needed for the synthesis include Zinc Nitrate Hexahydrate (HgmbG Chemicals), Thiourea (Sigma – Aldrich), Deionized water, and Ethylenediamine (ACROS Organics). All chemicals did not need further purification, as they were of analytical grade.

Synthesis of ZnS Nanoparticles

A 0.5 M solution of zinc nitrate hexahydrate ($Zn(NO_3)_2{\cdot}6H_2O$) (2.8404 g) and a 1.0 M solution of thiourea (CH_4N_2S) (2.2836 g) were prepared in a mixed solvent (30 mL) consisting of equal volumes (15 mL each) of deionized (DI) water and ethylenediamine ($H_2NCH_2CH_2NH_2$). The mixture was stirred for 30 minutes to ensure complete dissolution of the precursors. The resulting solution was transferred to a steel autoclave and sealed. The autoclave was then heated to 170 °C in a furnace oven and maintained at this temperature for 16 hours. After cooling the autoclave to room temperature, the

Corresponding author: Hassan Mustapha Junaidu
hassanmustapha0@gmail.com
Department of Science Education, Faculty of Technology Education Abubakar Tafawa Balewa University Bauchi, Nigeria.
© 2024. Faculty of Technology Education. ATBU Bauchi. All rights reserved

reaction mixture was centrifuged to separate the ZnS nanoparticles from the byproducts. The collected precipitate was washed sequentially with ethanol (once), DI water (three times), and ethanol (once again) to remove any impurities. The washed precipitate was dried in a drying oven at 60 °C for approximately 6 hours. The dried product was then ground using a mortar and pestle and stored as a powder in a sealed sample bottle for future characterization and use.

Reagents used for the Fabrication Process

CZTSe and ZnS synthesized via hydrothermal methods were employed in the fabrication of ultrathin CZTSe solar cells. Additionally, other materials such as TiO_2, ITO, and silver were utilized in the fabrication process.

Fabrication of the ITO/ TiO_2/ ZnS/ CZTSe/ Ag Photovoltaic Cell Device

The device fabrication commenced with the preparation of an indium tin oxide (ITO) coated conducting glass substrate. The ITO substrate underwent cleaning via sonication in a deionized (DI) water and acetone mixture for 5 minutes, followed by drying in an oven at 60 °C. This cleaning step removes surface contaminants that could hinder device performance. A compact titanium dioxide (TiO_2) layer, serving as the electron transport layer (ETL), was deposited onto the cleaned ITO substrate using a spin-coating technique. A drop of TiO_2 precursor solution was dispensed onto the substrate and spun at 2000 rpm for 120 seconds using a MIDAS spin coater system. Subsequent annealing at 250 °C for 5 minutes in a furnace completes the formation of the ETL.

Zinc sulfide (ZnS) powder was thermally evaporated onto the TiO_2 layer using an Edwards auto 306 thermal evaporators to create the buffer layer. This layer facilitates efficient charge transport between the ETL and the absorber layer. Following ZnS buffer layer deposition, CZTSe powder was similarly evaporated onto the structure using the thermal evaporator to form the light-absorbing layer. The CZTSe layer is responsible for photon absorption and exciton generation in the device. The fabricated device, consisting of the ITO/TiO_2/ZnS/CZTSe stack, underwent annealing in a furnace at 300 °C for 1 hour. This annealing step promotes film densification, improves interface quality, and potentially influences device performance. Finally, a silver (Ag) back contact was deposited onto the CZTSe layer using thermal evaporation to complete the solar cell structure. The back contact serves as the positive electrode for current collection.

Characterization

X-ray diffraction (XRD) analysis was performed using a Philips X' Pert pro Panalytical PW 3040 MPD X-ray diffractometer to determine the crystal structure and phase purity of the thin films within the device (ITO, TiO_2, ZnS, CZTSe). Atomic force microscopy (AFM) with a Bruker Dimension Edge AFM was employed to investigate the surface morphology and topography of the thin films. This analysis provides information about film roughness, uniformity, and potential presence of surface features. UV-visible (UV-Vis) spectroscopy was conducted using a Shimadzu UV-3600 model UV-Vis-NIR spectrophotometer over a wavelength range of 350-850 nm. This characterization enables the determination of the optical absorption coefficient and bandgap energy of the materials, crucial parameters for solar cell performance.

The electrical properties, specifically resistivity and conductivity, of the thin films were measured using a Keithley 236 source-measure unit. Understanding these properties is essential for analyzing charge transport within the device. The performance efficiency of the fabricated CZTSe/ZnS solar cell was evaluated under simulated solar illumination conditions. A solar simulator (TECC model 0.5) lamp, operating at 70 W and mimicking an air mass (AM) 1.5 global spectrum with an irradiance of 100 mW/cm², provided the simulated light source. Current density-voltage (J-V) characteristics were measured using an ADCMT 6243 DC voltage current source/monitor. The *I-V* data allows for the calculation of key solar cell parameters such as open-circuit voltage (*Voc*), short-circuit current (*Isc*), fill factor (*FF*), and efficiency.

Corresponding author: Hassan Mustapha Junaidu
✉ hassanmustapha0@gmail.com
Department of Science Education, Faculty of Technology Education Abubakar Tafawa Balewa University Bauchi, Nigeria.
© 2024. Faculty of Technology Education. ATBU Bauchi. All rights reserved

JOURNAL OF SCIENCE TECHNOLOGY AND EDUCATION 12(4), DECEMBER, 2024
ISSN: 2277-0011; Journal homepage: www.atbuftejoste.com.ng

RESULTS AND DISCUSSION

Structural and Morphological properties of the ZnS nanoparticles

XRD, FESEM and EDS analysis

The XRD patterns of the hydrothermally synthesized ZnS nanoparticles is presented in figure 1.

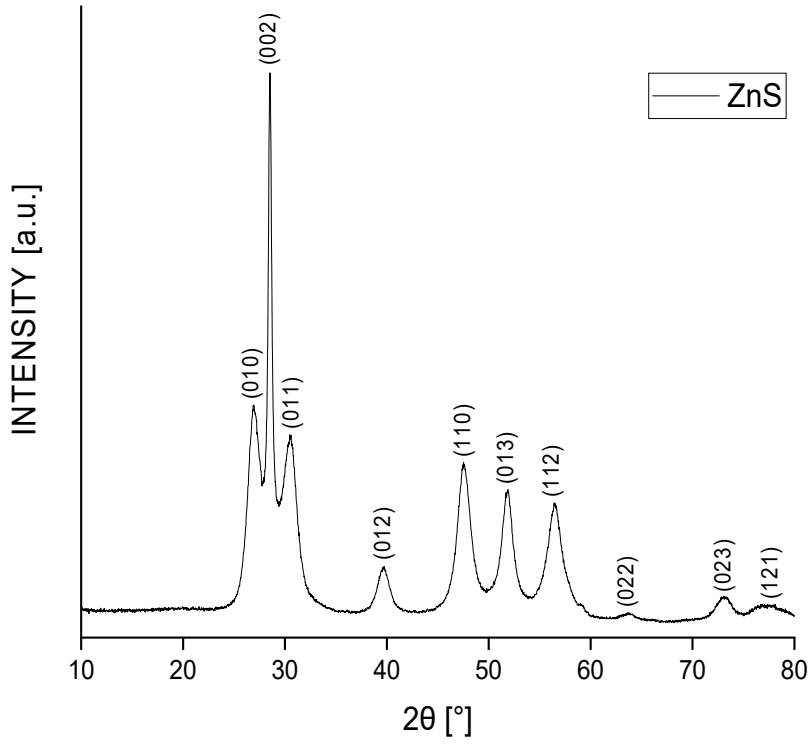

Figure 1: XRD pattern of the hydrothermally synthesized ZnS nanoparticles

The XRD pattern of the hydrothermally synthesized ZnS sample is presented in Figure 1. The pattern exhibits distinct diffraction peaks at 2θ values of 26.426°, 28.671°, 30.259°, 39.844°, 47.485°, 52.658°, 56.879°, 64.209°, 74.201°, and 78.603°. These peaks can be indexed to the (010), (002), (011), (012), (110), (013), (112), (022), (023), and (121) crystal planes of the wurtzite ZnS phase (ICSD ref code 98-007-1902). This confirms the successful synthesis of crystalline ZnS with a hexagonal crystal structure. The calculated lattice constants for the sample are a = 3.8230 Å and c = 6.2610 Å. These values are consistent with previously reported data for wurtzite ZnS Zhao & Zhang (2012) and Mendil et al. (2016) synthesized using similar solvothermal/ hydrothermal routes.

Figure 2 displays the energy-dispersive X-ray spectroscopy (EDS) analysis of the ZnS sample. The spectrum reveals the elemental composition of the material, with quantitative data indicating the weight percentage of each element present.

Corresponding author: Hassan Mustapha Junaidu
hassanmustapha0@gmail.com
Department of Science Education, Faculty of Technology Education Abubakar Tafawa Balewa University Bauchi, Nigeria.
© 2024. Faculty of Technology Education. ATBU Bauchi. All rights reserved

JOURNAL OF SCIENCE TECHNOLOGY AND EDUCATION 12(4), DECEMBER, 2024
ISSN: 2277-0011; Journal homepage: www.atbuftejoste.com.ng

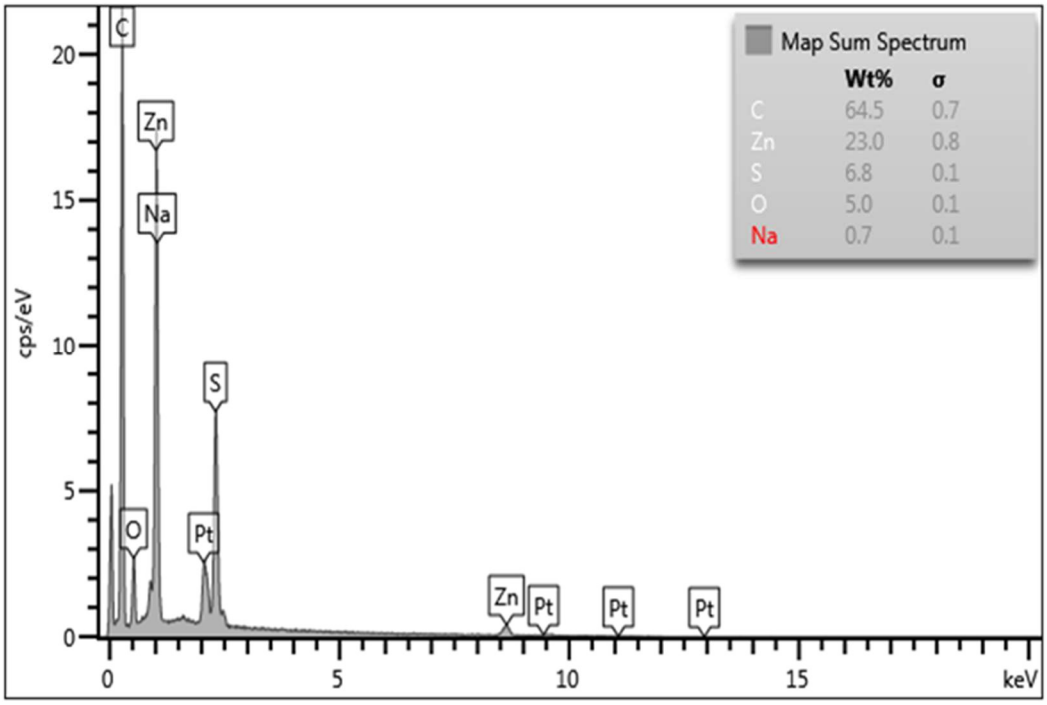

Figure 2: The map sum spectrum of the ZnS nanoparticles

Figure 2 presents the EDS analysis of the ZnS nanoparticles. The elemental composition is identified, with weight percentages of the elements with Carbon (C): 64.5%, Zinc (Zn): 23.0%, Sulfur (S): 6.8%, Oxygen (O): 5.0%, and Sodium (Na): 0.7% The high carbon (C) content (64.5%) likely originates from the carbon tape used to secure the sample during analysis. The presence of oxygen (O) at 5.0% might be due to surface oxidation or residual air in the measurement chamber.

While the EDS data provides weight percentages, the stoichiometric ratio of the compound is typically determined using atomic percentages. These values will be presented in Table 1.

Table 1: The atomic weight percentage of the ZnS nanoparticles

Element	At % composition	$\frac{[S]}{[Zn]}$
Zn	62.39	0.6
S	37.61	

Table 1 presents the quantitative elemental composition of the ZnS nanoparticles obtained from EDS analysis. The data reveals atomic percentages of 62.39% for Zinc (Zn) and 37.61% for Sulfur (S). This translates to a stoichiometric ratio of Zn:S close to 1.66:1, indicating a slight sulfur deficiency in the ZnS powder. The morphology of the ZnS nanoparticles is visualized using FESEM imaging, as presented in Figure 3.

Corresponding author: Hassan Mustapha Junaidu
✉ *hassanmustapha0@gmail.com*
Department of Science Education, Faculty of Technology Education Abubakar Tafawa Balewa University Bauchi, Nigeria.
© 2024. Faculty of Technology Education. ATBU Bauchi. All rights reserved

JOURNAL OF SCIENCE TECHNOLOGY AND EDUCATION 12(4), DECEMBER, 2024
ISSN: 2277-0011; Journal homepage: www.atbuftejoste.com.ng

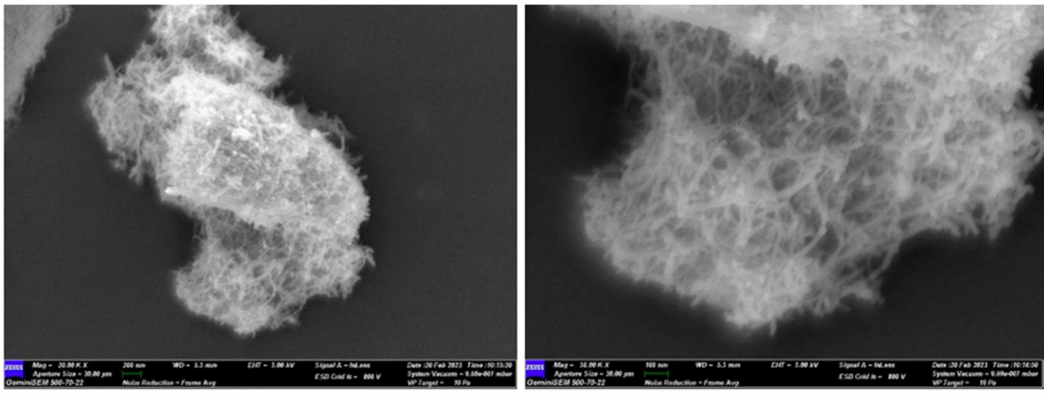

(a) 20.0 KX magnification (b) 50.0 KX magnification

Figure 3: FESEM images of the ZnS nanoparticles

SThe morphology of the hydrothermally synthesized ZnS nanoparticles is depicted in Figure 3. The FESEM images (Figures 3(a) and 3(b)) reveal that the ZnS consists of clusters of nanowires. These nanowires appear to be interconnected, forming one-dimensional (1D) nanostructures (Tiwari & Dhoble, 2017).

Structural and Morphological properties of the ZnS Thin film XRD and AFM of the ZnS thin film

Figure 4 presents the XRD patterns of ZnS nanoparticles prepared via thermal evaporation. The samples were prepared using different masses ranging from 0.002 g to 0.006 g and all underwent annealing at 180 °C for 1 hour.

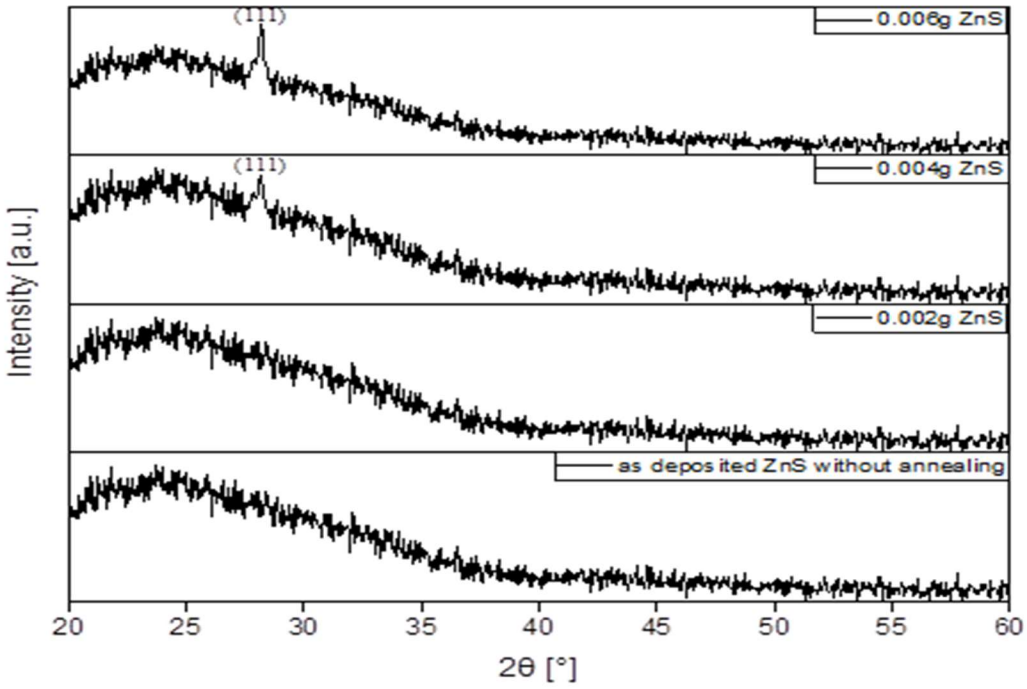

Corresponding author: Hassan Mustapha Junaidu
✉ *hassanmustapha0@gmail.com*
Department of Science Education, Faculty of Technology Education Abubakar Tafawa Balewa University Bauchi, Nigeria.
© 2024. Faculty of Technology Education. ATBU Bauchi. All rights reserved

JOURNAL OF SCIENCE TECHNOLOGY AND EDUCATION 12(4), DECEMBER, 2024
ISSN: 2277-0011; Journal homepage: www.atbuftejoste.com.ng

Figure 4: XRD patterns of annealed 180° C ZnS thin film, (from top to bottom) 0.006 g, 0.004 g, 0.002 g and as deposited without annealing ZnS thin film

Figure 4 displays the XRD patterns of ZnS thin films deposited via thermal evaporation with varying precursor masses (0.002 g to 0.006 g). All samples underwent annealing at 300 °C for 1 hour. The XRD patterns of the as-deposited thin film (without annealing) and the 0.002 g film exhibit no significant peaks, indicating an amorphous or poorly crystalline nature. In contrast, the 0.004 g and 0.006 g samples show distinct diffraction peaks, particularly at 2θ ≈ 28° corresponding to the (111) crystal plane of the cubic ZnS phase (ICSD ref code 98-009-1124). This observation matches the patterns reported by Benyahia et al. (2015) and (Deshmukh et al., 2016). The crystallite sizes of the 0.006 g and 0.004 g films were calculated using the Scherrer relation $D = \frac{K\lambda}{\beta Cos\theta}$ (Scherrer, 1918), where D is the crystallite size, K is the Scherrer constant given by 0.9, λ is the x – ray wavelength for CuK_α = 1.5406 Å, β is the full – width at half maximum (FWHM) and θ is the Bragg's angle, resulting in values of 22.48 nm and 19.12 nm, respectively. Additionally, the crystallinity indexes were determined to be 6.05% and 3.70%, respectively. These results suggest that a higher precursor mass (0.006 g) leads to increased film thickness and consequently, a higher degree of crystallinity. This trend aligns with observations reported by Bioki & Zarandi (2011) and Özakin et al. (2012). A summary of the key XRD findings can be presented in table 2.

Table 2: XRD results for different weights of the ZnS thin film

Weight of ZnS nanoparticles (g)	Peak plane	Peak position (2θ)	FHWM (β)	Crystallite size (nm)	Crystallinity index (%)
0.004	(111)	28.01	0.4284	19.12	3.70
0.006	(111)	28.21	0.3644	22.48	6.05

Figure 5 presents the AFM topography images of ZnS thin films deposited using varying precursor masses (0.002 g, 0.004 g, and 0.006 g) and annealed at 300 °C. The images (Figures 5(a) - (c)) reveal the surface morphology of the films at the nanoscale.

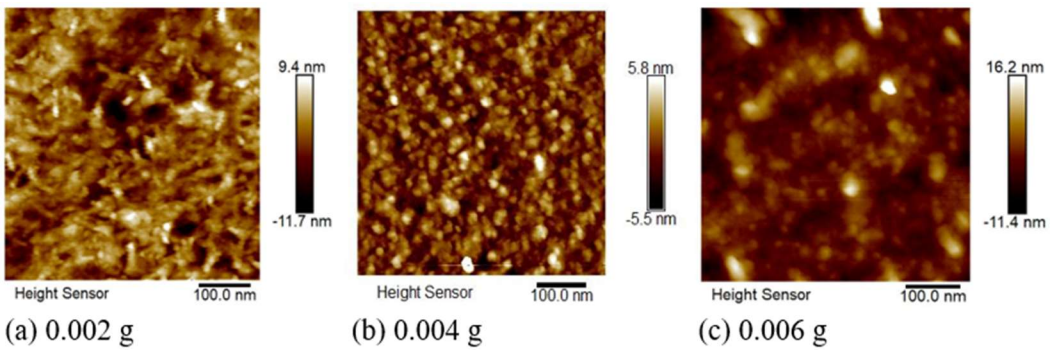

Figure 5: 2D height sensor topographical image of the ZnS thin film

Figure 5 (a)–(c) illustrates the topographical analysis of ZnS thin films deposited at varying mass loadings, revealing distinct morphological characteristics. Films prepared with 0.002 g of ZnS display small, irregularly shaped particles densely aggregated, with an average

Corresponding author: Hassan Mustapha Junaidu
✉ hassanmustapha0@gmail.com
Department of Science Education, Faculty of Technology Education Abubakar Tafawa Balewa University Bauchi, Nigeria.
© 2024. Faculty of Technology Education. ATBU Bauchi. All rights reserved

JOURNAL OF SCIENCE TECHNOLOGY AND EDUCATION 12(4), DECEMBER, 2024
ISSN: 2277-0011; Journal homepage: www.atbuftejoste.com.ng

diameter of 18.41 nm and a height of 6.30 nm within an area of 320.65 nm². Incrementing the mass loading to 0.004 g yields slightly larger, irregularly shaped particles sparsely distributed, measuring an average diameter of 21.06 nm and a height of 5.23 nm within an area of 426.16 nm². Films deposited with 0.006 g of ZnS exhibit larger, irregularly shaped particles dispersed, with an average diameter of 28.17 nm and a height of 10.55 nm within an area of 765.06 nm². Moreover, film thickness analysis reveals approximate values of 9.47 nm, 19.90 nm, and 22.25 nm for mass loadings of 0.002 g, 0.004 g, and 0.006 g, respectively.

The AFM investigation of ZnS thin films (Figure 5) underscores a discernible trend. As the quantity of ZnS nanoparticles employed for deposition escalates (from 0.002 g to 0.006 g), both the average particle size (18.41 nm to 28.17 nm) and film thickness (9.47 nm to 22.25 nm) proportionately increase. This observation suggests a direct correlation between precursor mass and the resultant properties of the thin film. The augmented particle size may be attributed to enhanced crystallinity concomitant with increased film thickness. Table 3 succinctly encapsulates these AFM findings for future reference.

Table 3: Summary of the AFM results of the ZnS thin film

Weight of ZnS nanoparticles (g)	Thickness (nm)	Particle diameter (nm)	Particle height (nm)	Surface area (nm²)
0.002	9.47	18.41	6.30	320.65
0.004	19.90	21.06	5.23	426.16
0.006	22.25	28.17	10.55	765.06

Optical and Electrical properties of the ZnS Thin film UV – Vis of the ZnS thin film

The bandgap energies of the 0.002 g, 0.004 g and 0.006 g ZnS thin films are presented in figure 6.

Figure 6: The bandgap energies of the 0.002 g, 0.004 g, and 0.006 g ZnS thin films

Corresponding author: Hassan Mustapha Junaidu
hassanmustapha0@gmail.com
Department of Science Education, Faculty of Technology Education Abubakar Tafawa Balewa University Bauchi, Nigeria.
© 2024. Faculty of Technology Education. ATBU Bauchi. All rights reserved

JOURNAL OF SCIENCE TECHNOLOGY AND EDUCATION 12(4), DECEMBER, 2024
ISSN: 2277-0011; Journal homepage: www.atbuftejoste.com.ng

Figure 6 presents the band gap energy values for ZnS thin films deposited with varying thicknesses (0.002 g, 0.004 g, and 0.006 g).

The bandgap energies were deduced using the Tauc relation (Wooten, 1972), $\alpha h\upsilon = B(h\upsilon - E_g)^n$. Where α is absorption coefficient, *B* is the Tauc's constant, E_g is the band gap energy and *n* is an integer with value $\frac{1}{2}$, and 2 for indirect allowed and direct allowed transitions respectively. To determine the band gap energy, a graph $(\alpha h\upsilon)^2$ vs $h\upsilon$ is plotted, and an extrapolation is done on the linear region of the $(\alpha h\upsilon)^2$ axis and its intercept with the $h\upsilon$ axis is the band gap energy. The data reveals a decreasing trend in band gap energy as the film thickness increases. Specifically, the band gap energy decreases from 3.87 eV for the 0.002 g film to 3.83 eV for the 0.006 g film. This observation aligns with the findings reported by Bioki & Zarandi (2011). The summary of the bandgap energy is given in table 4.

Table 4: Summary of the bandgap energy of the ZnS thin film

Weight of deposited ZnS nanoparticles (g)	Thickness of ZnS thin film (nm)	Bandgap energy (eV)
0.002	9.47	3.90
0.004	19.90	3.94
0.006	22.25	3.98

Resistivity, Sheet Resistance and Conductivity Results of the ZnS thin films

Four-probe measurements were employed to determine the electrical conductivity of the ZnS thin films deposited with varying thicknesses (0.002 g, 0.004 g, and 0.006 g). Voltages (mV) were measured across a defined range of applied currents (-0.01 mA to +0.01 mA). These measurements were then used to plot the corresponding voltage-current (*V-I*) characteristics for each film, as presented in Figure 7. By analyzing the slope and other features of the V-I curves, the resistivity, sheet resistance and conductivity of the ZnS thin films were obtained.

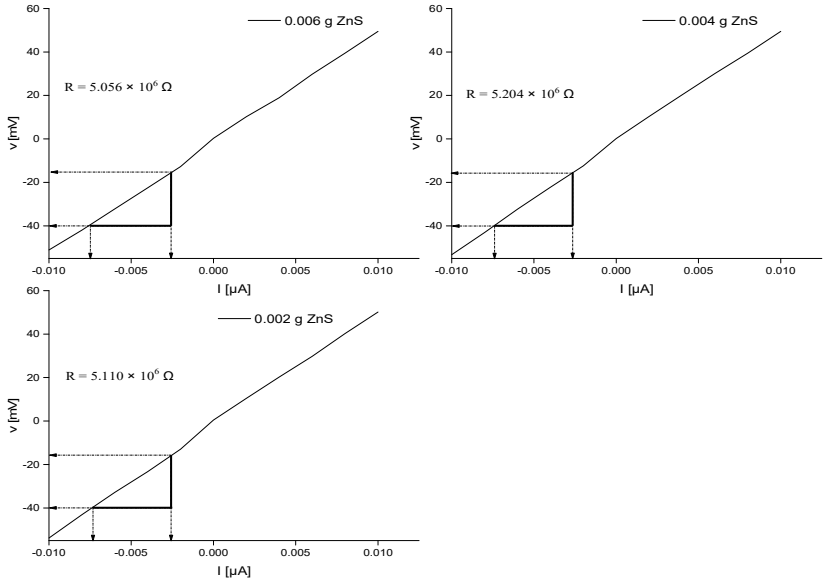

Figure 7: Graphs of resistance of the 0.006 g, 0.004 g and 0.002 g ZnS thin films

Corresponding author: Hassan Mustapha Junaidu
hassanmustapha0@gmail.com
Department of Science Education, Faculty of Technology Education Abubakar Tafawa Balewa University Bauchi, Nigeria.
© 2024. Faculty of Technology Education. ATBU Bauchi. All rights reserved

JOURNAL OF SCIENCE TECHNOLOGY AND EDUCATION 12(4), DECEMBER, 2024
ISSN: 2277-0011; Journal homepage: www.atbuftejoste.com.ng

Analysis of the V-I curves reveals several key findings about the electrical properties of the ZnS thin films. The resistance values are: 5.06 × 10^6 Ω for the 0.006 g film, 5.20 × 10^6 Ω for the 0.004 g film, and 5.11 × 10^6 Ω for the 0.002 g film. Using the formular $\rho = \frac{\pi}{ln2} \times R \times t \times k$ (Keithley Instruments Inc., 2005), where ρ is volume resistivity (Ω-cm), *R* is resistance (Ω), *t* is sample thickness (cm) and *k* is the correction factor, these resistance values translate to resistivities of 2.2 × 10^1 Ω-cm for the 0.002 g film, 4.6 × 10^1 Ω-cm for the 0.004 g film, and 5.0 × 10^1 Ω-cm for the 0.006 g film.

The sheet resistance R_s, can be calculated from the relation $R_s = \frac{\rho}{T}$, where ρ is the resistivity and T is the thickness of the thin film, thus the sheet resistance follows a similar trend: 2.27 × 10^9 Ω for the 0.002 g film, 2.31 × 10^9 Ω for the 0.004 g film, and 2.23 × 10^9 Ω for the 0.006 g film. In terms of conductivity, deduced from the relation $\sigma = \frac{1}{\rho}$, where σ is conductivity and ρ is resistivity, the 0.002 g film exhibits the highest value at 4.7 × 10^{-2} S/cm, followed by the 0.006 g film at 2.0 × 10^{-2} S/cm and the 0.004 g film at 2.2 × 10^{-2} S/cm. A more comprehensive summary of these electrical properties can be found in table 5.

Table 5: Summary of the electrical properties of the ZnS thin film

Weight of deposited ZnS nanoparticles (g)	Resistance × 10^6 (Ω)	Resistivity × 10^1 (Ω-cm)	Sheet resistance × 10^9 (Ω)	Conductivity × 10^{-2} S/cm
0.002	5.11	2.20	2.27	4.7
0.004	5.20	4.60	2.31	2.2
0.006	5.06	5.00	2.23	2.0

The Fabricated ITO/ TiO_2/ ZnS/ CZTSe/ Ag Solar cell

The cell structure, illustrated schematically in figure 8, incorporate layers of ITO/ TiO_2/ ZnS/ CZTSe/ Ag. Notably, all the fabricated films fall under the category of ultrathin films, with thicknesses around 300 nm. This classification aligns with the definition where films below 700 nm are considered ultrathin (Gezgin et al., 2021).

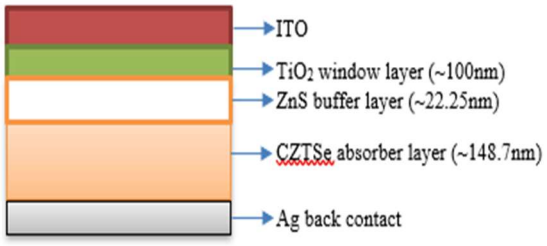

Figure 8: Schematic diagram of the ITO/ TiO_2/ ZnS/ CZTSe/ Ag photovoltaic cell

XRD and AFM of the ITO/ TiO_2/ ZnS/ CZTSe/ Ag photovoltaic cell device

The XRD analysis of the ITO/ TiO_2/ ZnS/ CZTSe/ Ag photovoltaic cell device is presented in figure 9:

Corresponding author: Hassan Mustapha Junaidu
✉ hassanmustapha0@gmail.com
Department of Science Education, Faculty of Technology Education Abubakar Tafawa Balewa University Bauchi, Nigeria.
© 2024. Faculty of Technology Education. ATBU Bauchi. All rights reserved

JOURNAL OF SCIENCE TECHNOLOGY AND EDUCATION 12(4), DECEMBER, 2024
ISSN: 2277-0011; Journal homepage: www.atbuftejoste.com.ng

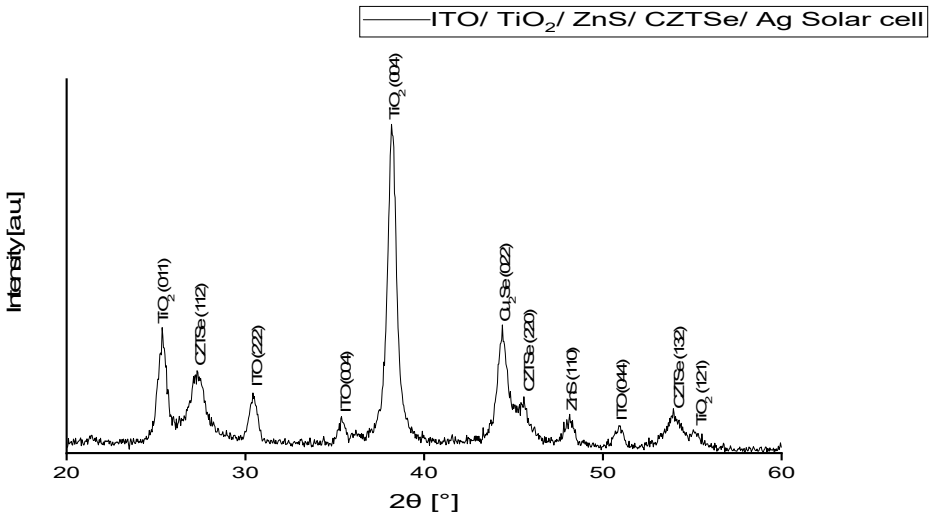

Figure 9: XRD pattern of the ITO/ TiO_2/ ZnS/ CZTSe/ Ag photovoltaic cell device

The X-ray diffraction (XRD) pattern of the fabricated photovoltaic cell device (Figure 9) confirms the presence of all deposited thin film layers. The observed peaks can be attributed to the following materials and crystallographic phases: CZTSe (Copper Zinc Tin Sulfide Selenide): Peaks at 2θ = 27.35°, 45.17°, and 53.6° correspond to the (112), (220), and (132) diffraction planes of the tetragonal kesterite structure (ICSD reference code: 98-006-7242). ZnS (Zinc Sulfide): Peaks at 2θ = 26.41° and 47.45° correspond to the (010) and (110) planes of the hexagonal wurtzite structure (ICSD reference code: 98-010-8169). TiO_2 (Titanium Dioxide): Peaks at 2θ = 25.33° and 37.88° correspond to the (011) and (004) diffraction planes of the tetragonal structure (ICSD reference code: 98-004-5260). ITO (Indium Tin Oxide): The most prominent peaks at 2θ = 30.44°, 35.31°, and 51.0° correspond to the (222), (004), and (044) planes of the cubic structure (ICSD reference code: 98-005-1986). Secondary Phase: A weak peak at 2θ = 44.14° indicates the presence of a secondary phase, Cu_2Se, with the (022) diffraction plane. The AFM topographical image of the ITO/ TiO_2/ ZnS/ CZTSe/ Ag photovoltaic cell device is shown in Figure 9 (a) and (b).

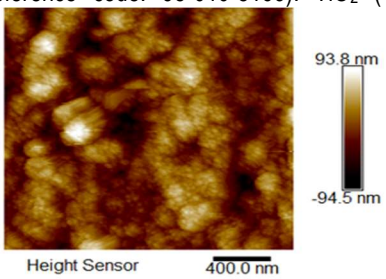

(a) 2D height sensor topographical image of the ITO/ TiO_2/ ZnS/ CZTSe/ Ag photovoltaic cell device

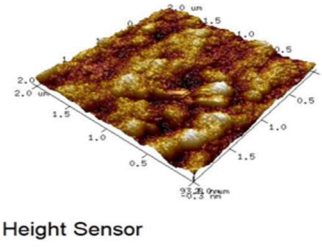

(b) 3D topographical image of the ITO/ TiO_2/ ZnS/ CZTSe/ Ag photovoltaic cell device

Figure 9: AFM images of the ITO/ TiO_2/ ZnS/ CZTSe/ Ag photovoltaic cell device

Atomic force microscopy (AFM) analysis of the photovoltaic cell device (Figure 9(a) and (b)) reveals large, irregularly shaped particles. These particles are densely packed with

Corresponding author: Hassan Mustapha Junaidu
✉ hassanmustapha0@gmail.com
Department of Science Education, Faculty of Technology Education Abubakar Tafawa Balewa University Bauchi, Nigeria.
© 2024. Faculty of Technology Education. ATBU Bauchi. All rights reserved

large voids separating them. The analysis indicates an average particle size of 117.35 nm in diameter and 31.80 nm in height, measured within an area of 22,976.35 nm². The surface roughness analysis shows a root mean square (RMS) average height deviation (Rq) of 0.027 µm and an arithmetic average (Ra) of the surface height deviation of 0.022 µm. A summary of these AFM findings can be found in Table 6.

Table 6: Summary of the AFM results of the ITO/ TiO_2/ ZnS/ CZTSe/ Ag photovoltaic cell device

Particle diameter (nm)	Particle height (nm)	Area (nm²)	Root mean square average of heigh deviation (µm)	Arithmetic average of the absolute values of the surface height deviation (µm)
117.35	31.80	22,976.35	0.027	0.022

I – V characteristics Results of the ITO/ TiO_2/ ZnS/ CZTSe/ Ag Photovoltaic Cell Device

The I – V characteristics curve of the ITO/ TiO_2/ ZnS/ CZTSe/ Ag photovoltaic cell device is presented in figure 10.

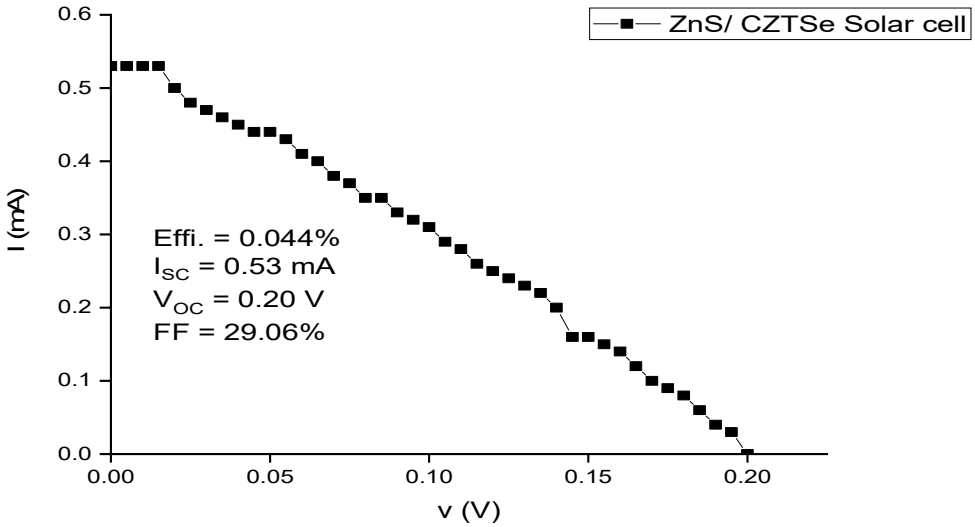

Figure 10: The I – V characteristics curve of the ITO/ TiO_2/ ZnS/ CZTSe/ Ag photovoltaic cell device

The fabricated photovoltaic cell device (Figure 10) exhibited a power conversion efficiency (η) of 0.044%, along with a short-circuit current (*Isc*) of 0.53 mA, open-circuit voltage (*Voc*) of 0.20 V, and fill factor (*FF*) of 29.06%. While this efficiency is low, it demonstrates the potential of ZnS as a possible n-type buffer layer for the p-type CZTSe absorber layer, unlike previous findings by Barkhouse et al. (2012) where no efficiency was observed with a ZnS buffer. Several factors might contribute to the low efficiency such as the device utilizing ultrathin films, known for their low photon absorption rate due to their thinness. This likely resulted in the low Isc, as fewer photons are generated for absorption. Park et al., (2017) achieved higher efficiency for CZTSSe absorbers

Corresponding author: Hassan Mustapha Junaidu
✉ hassanmustapha0@gmail.com
Department of Science Education, Faculty of Technology Education Abubakar Tafawa Balewa University Bauchi, Nigeria.
© 2024. Faculty of Technology Education. ATBU Bauchi. All rights reserved

with optimized ZnS buffer layer thickness. The ultrathin ZnS layer in this device might not be optimal. Hernández-Calderón et al. (2020) suggest that ultrathin buffer layers can introduce pinholes, hindering electrical properties.

Additionally, Barkhouse et al. (2012) reported a high spike-like band offset at the ZnS/CZTSe interface for thicker ZnS layers. Such high spikes can significantly reduce Isc by creating a barrier for electron movement (Neuschitzer et al., 2016). This high band offset between the ZnS and CZTSe layers could be another factor limiting Isc and overall efficiency. The ultrathin nature of the device might introduce porosity, potentially causing leakage of other layers into the CZTSe and leading to current leakage issues, as suggested by Ismail et al. (2014). Fabricating a pinhole-free buffer layer below 25 nm is also very challenging (Haghighi et al., 2018).

The presence of a Cu_2Se secondary phase, observed in the XRD analysis, can negatively impact performance by affecting the cell's electronic properties, as noted by Just et al. (2016). Lai et al. (2023) further explain that Cu2Se secondary phases in CZTSe films create leakage paths that hinder device interfaces. This study used TiO_2 as the window layer instead of the conventional ZnO used in kesterite-based photovoltaic cells. While TiO_2 offers a high conduction band edge, it can also enhance electron-hole pair recombination during electron transfer from the absorber layer to the ITO substrate (Sun et al., 2020). This recombination generally reduces cell performance by impeding the short-circuit current. Table 7 summarizes the performance parameters of the device.

Table 7: Summary of the performance efficiency of the ITO/ TiO_2/ ZnS/ CZTSe/ Ag photovoltaic cell device

Short circuit current	Open circuit voltage	Fill factor	Max power (max Voc × max Jsc)	Input power	Conversion efficiency
0.53	0.2	29.06	0.0308	70	0.044

CONCLUSION

In conclusion, this study elucidates the potential of Zinc Sulfide (ZnS) as a viable alternative to Cadmium Sulfide (CdS) in thin-film photovoltaic applications, particularly in Copper Zinc Tin Selenide (CZTSe) solar cells. Through comprehensive investigations encompassing synthesis techniques, structural characterization, morphological analysis, and device fabrication, significant insights have been gained.

The synthesis of ZnS nanoparticles via hydrothermal methods yielded promising results, with X-ray diffraction (XRD) confirming the formation of well-defined wurtzite crystal structures. Scanning electron microscopy (SEM) images revealed the morphological characteristics of ZnS nanoparticles, showcasing their potential for thin-film applications. Additionally, the optical properties of ZnS thin films were found to be tunable with varying thicknesses, suggesting flexibility in bandgap engineering.

Integration of ZnS buffer layers into CZTSe solar cell devices demonstrated encouraging results, albeit with some performance trade-offs compared to CdS-based counterparts. While the efficiency of ZnS-buffered CZTSe devices was lower, the study highlights the feasibility of ZnS as a non-toxic and environmentally sustainable buffer layer material. Electrical characterization revealed promising conductivity properties of ZnS thin films, laying the groundwork for further optimization and improvement.

Overall, this research contributes to advancing the field of thin-film photovoltaics by exploring alternative materials that address environmental concerns while maintaining device performance. Further optimization and refinement of ZnS-based CZTSe solar cells hold promise for realizing efficient and eco-friendly solar energy technologies, contributing to the global transition towards sustainable energy solutions.

Corresponding author: Hassan Mustapha Junaidu
✉ hassanmustapha0@gmail.com
Department of Science Education, Faculty of Technology Education Abubakar Tafawa Balewa University Bauchi, Nigeria.
© 2024. Faculty of Technology Education. ATBU Bauchi. All rights reserved

REFERENCES

Barkhouse, D. A. R., Haight, R., Sakai, N., Hiroi, H., Sugimoto, H., & Mitzi, D. B. (2012). Cd-free buffer layer materials on Cu 2ZnSn(S xSe 1-x) 4: Band alignments with ZnO, ZnS, and In 2S 3. *Applied Physics Letters*, *100*(19). https://doi.org/10.1063/1.4714737

Barman, B., & Kalita, P. K. (2020). Theoretical Investigation on Performance Enhancement of CIGS Based Solar Cells. *Journal of Nano- and Electronic Physics*, *12*(6), 06036-1-06036–4. https://doi.org/10.21272/jnep.12(6).06036

Bashar, M. S., Matin, R., Sultana, M., Siddika, A., Rahaman, M., Gafur, M. A., & Ahmed, F. (2020). Effect of rapid thermal annealing on structural and optical properties of ZnS thin films fabricated by RF magnetron sputtering technique. *Journal of Theoretical and Applied Physics*, *14*(1), 53–63. https://doi.org/10.1007/s40094-019-00361-5

Benyahia, K., Benhaya, A., & Aida, M. S. (2015). ZnS thin films deposition by thermal evaporation for photovoltaic applications. *Journal of Semiconductors*, *36*(10). https://doi.org/10.1088/1674-4926/36/10/103001

Bioki, H. A., & Zarandi, M. B. (2011). Effects of Annealing and Thickness on the Structural and Optical Properties of Crystalline ZnS Thin Films Prepared by PVD Method. In *International Journal of Optics and Photonics (IJOP)* (Vol. 5, Issue 2).

Chantana, J., Kato, T., Sugimoto, H., & Minemoto, T. (2017). Thin-film Cu(In,Ga)(Se,S)2-based solar cell with (Cd,Zn)S buffer layer and Zn1−xMgxO window layer. *Progress in Photovoltaics: Research and Applications*, *25*(6), 431–440. https://doi.org/10.1002/pip.2879

Chantana, J., Kato, T., Sugimoto, H., & Minemoto, T. (2018). Heterointerface recombination of Cu(In,Ga)(S,Se)2-based solar cells with different buffer layers. *Progress in Photovoltaics: Research and Applications*, *26*(2), 127–134. https://doi.org/10.1002/pip.2952

Delgado-Sanchez, J. M., & Lillo-Bravo, I. (2022). High Vapor Transport Deposition: A Novel Process to Develop Cu2ZnSn(SxSe1–x)4 Thin Film Solar Cells. *Solar RRL*, *6*(2). https://doi.org/10.1002/solr.202100835

Deshmukh, S. G., Jariwala, A., Agarwal, A., Patel, C., Panchal, A. K., & Kheraj, V. (2016). ZnS nanostructured thin-films deposited by successive ionic layer adsorption and reaction. *AIP Conference Proceedings*, *1724*. https://doi.org/10.1063/1.4945153

Diguna, L. J., Fitriani, A. D., Liasari, B. R., Timuda, G. E., Widayatno, W. B., Wismogroho, A. S., Zeng, S., Birowosuto, M. D., & Amal, M. I. (2021). Optical and photodetection properties of zno nanoparticles recovered from zn dross. *Crystals*, *11*(1), 1–8. https://doi.org/10.3390/cryst11010006

Eisa, M. H., & Ahmed, A. A. (2021). Structural characterization of synthesized Al-doped ZnS nanoparticles deposited on glass substrate. *Chalcogenide Letters*, *18*(12), 783–789. https://doi.org/10.15251/cl.2021.1812.783

Friedlmeier, T. M. /, Wieser, N. /, Walter, T. /, & Schock, H.-W. (1997). Heterojunctions Based on Cu~2ZnSnS~4 and Cu~2ZnSnSe~4 Thin Films (English). In *European photovoltaic solar energy conference*. https://www.tib.eu/en/search/id/BLCP:CN023425275/Heterojunctions-Based-on-Cu~2ZnSnS~4-and-Cu~2ZnSnSe~4?cHash=85fa1f2d94f7dd48648a1b8a11f22e16

Corresponding author: Hassan Mustapha Junaidu
✉ *hassanmustapha0@gmail.com*
Department of Science Education, Faculty of Technology Education Abubakar Tafawa Balewa University Bauchi, Nigeria.
© 2024. Faculty of Technology Education. ATBU Bauchi. All rights reserved

Gezgin, S. Y., Houimi, A., Mercimek, B., & Kiliç, H. Ş. (2021). The Effect of CZTS Ultrathin Film Thickness on the Electrical Characteristic of CZTS/Si Heterojunction Solar Cells in the Darkness and under the Illumination Conditions. *Silicon*, *13*(10), 3555–3567. https://doi.org/10.1007/s12633-020-00847-x

Goktas, A., Aslan, F., Yasar, E., & Mutlu, I. H. (2012). Preparation and characterisation of thickness dependent nano-structured ZnS thin films by sol-gel technique. *Journal of Materials Science: Materials in Electronics*, *23*(7), 1361–1366. https://doi.org/10.1007/s10854-011-0599-z

Haghighi, M., Minbashi, M., Taghavinia, N., Kim, D. H., Mahdavi, S. M., & Kordbacheh, A. A. (2018). A modeling study on utilizing SnS2 as the buffer layer of CZT(S, Se) solar cells. *Solar Energy*, *167*, 165–171. https://doi.org/10.1016/j.solener.2018.04.010

Hernández-Calderón, V., Vigil-Galán, O., Guc, M., Carrillo-Osuna, A., Ramírez-Velasco, S., Sánchez-Rodríguez, F. J., Vidal-Fuentes, P., Giraldo, S., Saucedo, E., & Sánchez, Y. (2020). CdS/ZnS Bilayer Thin Films Used As Buffer Layer in 10%-Efficient Cu2ZnSnSe4Solar Cells. *ACS Applied Energy Materials*, *3*(7), 6815–6823. https://doi.org/10.1021/acsaem.0c00937

Hsieh, W. M., Cheng, K. W., & Lue, S. J. (2011). Preparation and Characterization of ZnS Thin Films Using Chemical Bath Deposition Method: Effects of Deposition Time and Thermal Treatment. In *Supplemental Proceedings: Materials Fabrication, Properties, Characterization, and Modeling* (Vol. 2, pp. 43–50). John Wiley and Sons Inc. https://doi.org/10.1002/9781118062142.ch5

Huang, T. J., Yin, X., Qi, G., & Gong, H. (2014). CZTS-based materials and interfaces and their effects on the performance of thin film solar cells. *Physica Status Solidi - Rapid Research Letters*, *8*(9), 735–762. https://doi.org/10.1002/pssr.201409219

Ismail, A., Cho, J. W., Park, S. J., Hwang, Y. J., & Min, B. K. (2014). Synthesis of solution-processed Cu2ZnSnSe4 thin films on transparent conducting oxide glass substrates. *Bulletin of the Korean Chemical Society*, *35*(7), 1985–1988. https://doi.org/10.5012/bkcs.2014.35.7.1985

Ito, K., & Nakazawa, T. (1988). Electrical and Optical Properties of Stannite - Type Quaternary Semiconductor Thin films. *Japanese Journal of Applied Sciences*, *27*(11), 2094–2097.

Just, J., Sutter-Fella, C. M., Lützenkirchen-Hecht, D., Frahm, R., Schorr, S., & Unold, T. (2016). Secondary phases and their influence on the composition of the kesterite phase in CZTS and CZTSe thin films. *Physical Chemistry Chemical Physics*, *18*(23), 15988–15994. https://doi.org/10.1039/c6cp00178e

Keithley Instruments Inc. (2005). *Measuring the Resistivity and Determining the Conductivity Type of Semiconductor Materials Using a Four-Point Collinear Probe and the Model 6221 DC and AC Current Source Application Note Series*.

Kumar, S., & Arora, S. (2021). Effect of Buffer Layer on Cu (In, Ga)Se2 Solar Cell Performance. *SKIT Research Journal*, *11*(3), 20. https://doi.org/10.47904/ijskit.11.3.2021.20-24

Lai, F. I., Yang, J. F., Hsu, Y. C., & Kuo, S. Y. (2020). Sustainable Cu2ZnSnSe4 photovoltaic cells fabricated with a sputtered CdS buffer layer. *Progress in Photovoltaics: Research and*

Corresponding author: Hassan Mustapha Junaidu
✉ *hassanmustapha0@gmail.com*
Department of Science Education, Faculty of Technology Education Abubakar Tafawa Balewa University Bauchi, Nigeria.
© 2024. Faculty of Technology Education. ATBU Bauchi. All rights reserved

Applications, *28*(10), 1012–1023. https://doi.org/10.1002/pip.3307

Lai, F. I., Yang, J. F., Hsu, Y. C., & Kuo, S. Y. (2022). Suppressing the formation of double-layer in Cu2ZnSnSe4(CZTSe) absorber layer by facile heating process through nontoxic selenium atmosphere. *International Journal of Energy Research*, *46*(3), 3686–3696. https://doi.org/10.1002/er.7334

Lai, F.-I., Yang, J.-F., Chen, W.-C., Hsu, Y.-C., & Kuo, S.-Y. (2023). All-Vacuum-Deposited Bifacial Cu2ZnSnSe4 Photovoltaic Cells with Sputtered Cd-Free Buffer Layer. *International Journal of Energy Research*, *2023*, 1–17. https://doi.org/10.1155/2023/9215680

Li, J., Zhang, Y., Zhao, W., Nam, D., Cheong, H., Wu, L., Zhou, Z., & Sun, Y. (2015). A temporary barrier effect of the alloy layer during selenization: Tailoring the thickness of MoSe2 for efficient Cu2ZnSnSe4 solar cells. *Advanced Energy Materials*, *5*(9). https://doi.org/10.1002/aenm.201402178

Mendil, R., Ben Ayadi, Z., Ben Belgacem, J., & Djessas, K. (2016). The properties of ZnS thin films prepared by rf-magnetron sputtering from nanoparticles synthesized by solvothermal/hydrothermal route. *Journal of Materials Science: Materials in Electronics*, *27*(1), 444–451. https://doi.org/10.1007/s10854-015-3772-y

Mohammed, R. Y. (2021). Annealing effect on the structure and optical properties of cbd-zns thin films for windscreen coating. *Materials*, *14*(22). https://doi.org/10.3390/ma14226748

Nemade, K. R., & Waghuley, S. A. (2016). Ultra-violet C absorption and LPG sensing study of zinc sulphide nanoparticles deposited by a flame-assisted spray pyrolysis method. *Journal of Taibah University for Science*, *10*(3), 437–441. https://doi.org/10.1016/j.jtusci.2015.07.003

Neuschitzer, M., Lienau, K., Guc, M., Barrio, L. C., Haass, S., Prieto, J. M., Sanchez, Y., Espindola-Rodriguez, M., Romanyuk, Y., Perez-Rodriguez, A., Izquierdo-Roca, V., & Saucedo, E. (2016). Towards high performance Cd-free CZTSe solar cells with a ZnS(O,OH) buffer layer: The influence of thiourea concentration on chemical bath deposition. *Journal of Physics D: Applied Physics*, *49*(12). https://doi.org/10.1088/0022-3727/49/12/125602

Opasanont, B., Van, K. T., Kuba, A. G., Choudhury, K. R., & Baxter, J. B. (2015). Adherent and conformal Zn(S,O,OH) thin films by rapid chemical bath deposition with hexamethylenetetramine additive. *ACS Applied Materials and Interfaces*, *7*(21), 11516–11525. https://doi.org/10.1021/acsami.5b02482

Özakin, O., Güzeldir, B., Yildirim, M. A., Sağlam, M., & Ateş, A. (2012). Influence of film thickness on structural and optical properties of ZnS thin films obtained by SILAR method and analysis of Zn/ZnS/n-GaAs/In sandwich structure. *Physica Status Solidi (A) Applications and Materials Science*, *209*(4), 687–693. https://doi.org/10.1002/pssa.201127543

Park, J. Y., Chalapathy, R. B. V., Lokhande, A. C., Hong, C. W., & Kim, J. H. (2017). Fabrication of earth abundant Cu2ZnSnSSe4(CZTSSe) thin film solar cells with cadmium free zinc sulfide (ZnS) buffer layers. *Journal of Alloys and Compounds*, *695*, 2652–2660. https://doi.org/10.1016/j.jallcom.2016.11.178

Primc, G., Brenčič, K., Mozetič, M., & Gorjanc, M. (2021). Recent advances in the plasma-assisted synthesis of zinc oxide

Corresponding author: Hassan Mustapha Junaidu
✉ *hassanmustapha0@gmail.com*
Department of Science Education, Faculty of Technology Education Abubakar Tafawa Balewa University Bauchi, Nigeria.
© 2024. Faculty of Technology Education. ATBU Bauchi. All rights reserved

nanoparticles. In *Nanomaterials* (Vol. 11, Issue 5). Multidisciplinary Digital Publishing Institute (MDPI). https://doi.org/10.3390/nano11051191

Rodríguez, C. A., Sandoval-Paz, M. G., Saavedra, R., Trejo-Cruz, C., De La Carrera, F., Aragon, L. E., Sirena, M., Delplancke, M. P., & Carrasco, C. (2016). Comprehensive study of growth mechanism and properties of low Zn content Cd1-xZnxS thin films by chemical bath. *Materials Research*, *19*(6), 1335–1343. https://doi.org/10.1590/1980-5373-MR-2015-0660

Sara, B., Baya, Z., & Zineb, B. (2018). Investigation of Cu(In, Ga)Se2 solar cell performance with non-cadmium buffer layer using TCAD-SILVACO. *Materials Science- Poland*, *36*(3), 514–519. https://doi.org/10.2478/msp-2018-0054

Scherrer, P. (1918). Determination of the size and internal structure of colloid particles using X-rays. *News from the Society of Sciences in Göttingen*, *2*, 96–100.

Shi, L., Pei, C., Xu, Y., & Li, Q. (2011). Template-directed synthesis of ordered single-crystalline nanowires arrays of Cu2ZnSnS4 and Cu2ZnSnSe4. *Journal of the American Chemical Society*, *133*(27), 10328–10331. https://doi.org/10.1021/ja201740w

Sun, Y., Gao, Y., Hu, J., Liu, C., Sui, Y., Lv, S., Wang, F., & Yang, L. (2020). Comparison of effects of ZnO and TiO2 compact layer on performance of perovskite solar cells. *Journal of Solid State Chemistry*, *287*. https://doi.org/10.1016/j.jssc.2020.121387

Tiwari, A., & Dhoble, S. J. (2017). Critical analysis of phase evolution, morphological control, growth mechanism and photophysical applications of zns nanostructures (zero-dimensional to three-dimensional): A review. In *Crystal Growth and Design* (Vol. 17, Issue 1, pp. 381–407). American Chemical Society. https://doi.org/10.1021/acs.cgd.6b01463

Wang, S., Jiang, Z., Shen, Z., Sun, Y., Guo, H., Wu, L., Zhang, J., Ao, J., Wang, H., & Zhang, Y. (2021). Promising Cd-free double buffer layer in CZTSSe thin film solar cells. *Science China Materials*, *64*(2), 288–295. https://doi.org/10.1007/s40843-020-1419-8

Wirunchit, S., & Koetniyom, W. (2023). ZnO Nanoparticles Synthesis and Characterization by Hydrothermal Process for Biological Applications. *Physica Status Solidi (A) Applications and Materials Science*, *220*(10). https://doi.org/10.1002/pssa.202200364

Wooten, F. (1972). *OPTICAL PROPERTIES OF SOLIDS*.

Yassine, B., Tahar, B., & Fathi, G. (2022). Modeling and simulation of CZTS based solar cells with ZnS buffer layer and ZnO:F as a window layer using SCAPS-1D. *Chalcogenide Letters*, *19*(8), 503–511. https://doi.org/10.15251/CL.2022.198.503

Zhang, H., Cheng, S., Yu, J., Zhou, H., & Jia, H. (2016). Prospects of Zn(O,S) as an alternative buffer layer for Cu2ZnSnS4 thin-film solar cells from numerical simulation. *Micro and Nano Letters*, *11*(7), 386–390. https://doi.org/10.1049/mnl.2016.0130

Zhao, J. G., & Zhang, H. H. (2012). Hydrothermal synthesis and characterization of ZnS hierarchical microspheres. *Superlattices and Microstructures*, *51*(5), 663–667. https://doi.org/10.1016/j.spmi.2012.02.004

Corresponding author: Hassan Mustapha Junaidu
✉ *hassanmustapha0@gmail.com*
Department of Science Education, Faculty of Technology Education Abubakar Tafawa Balewa University Bauchi, Nigeria.
© 2024. Faculty of Technology Education. ATBU Bauchi. All rights reserved